AFFDL-TR-67-93

EFFECTS OF GUST VELOCITY SPATIAL DISTRIBUTIONS ON LATERAL-DIRECTIONAL RESPONSE OF A VTOL AIRCRAFT

ROBERT L. SWAIM, PhD

ALONZO J. CONNORS

FOREWORD

This report was prepared by Dr. Robert L. Swaim and Mr. Alonzo J. Connors of the Control Criteria Branch (FDCC), Flight Control Division, Air Force Flight Dynamics Laboratory. The research was initiated under Project No. 8219, "Stability and Control Investigations," Task No. 821903, "Flight Control Data." The work was administered by the Air Force Flight Dynamics Laboratory, Directorate of Laboratories, Air Force Systems Command, Wright-Patterson Air Force Base, Ohio.

The research was conducted during the period October 1965 through February 1967. This report was submitted by the authors March 1967.

The authors gratefully acknowledge the expert digital computer programming support of Mr. George Schubert of the Air Force Flight Dynamics Laboratory.

This technical report has been reviewed and is approved.

C. B. Westbrook

C. B. WESTBROOK
Chief, Control Criteria Branch
Flight Control Division
Air Force Flight Dynamics Laboratory

ABSTRACT

The effects of spanwise distribution of longitudinal and vertical components of gust velocity and longitudinal distribution of the lateral component on the lateral-directional response of a hovering VTOL aircraft are analyzed. Results show that spanwise effects of the longitudinal and vertical components are negligible, and the longitudinal distribution of the lateral component is significant in computing the power spectral densities of gust-induced side force, yawing moment, rolling moment, and the aircraft sideslip, yaw, and roll root-mean-square response angles. If the gust-induced angles of attack and sideslip angles are in the nonlinear range of lift curve slope, the above conclusions, which are based on linear aerodynamic theory, may not hold and an analysis based on momentum transfer of gust energy to the aircraft is recommended. Flow field interaction effects due to engine intake and exhaust also were not considered.

TABLE OF CONTENTS

ILLUSTRATIONS

NOMENCLATURE

b	wing span
C_{L_α}	wing lift curve slope
$C_{\ell\beta}$	rolling moment due to sideslip stability derivative
C_{ℓ_p}	rolling moment due to rolling velocity stability derivative
C_{ℓ_r}	rolling moment due to yawing velocity stability derivative
$C_{n\beta}$	yawing moment due to sideslip stability derivative
C_{n_p}	yawing moment due to rolling velocity stability derivative
C_{n_r}	yawing moment due to yawing velocity stability derivative
$C_{y\beta}$	side force due to sideslip stability derivative
C_{y_p}	side force due to rolling velocity stability derivative
C_{y_r}	side force due to yawing velocity stability derivative
$D\phi_g, D\psi_g$	equivalent rolling and yawing gust gradients
g	acceleration of gravity
I_x, I_z, I_{xz}	moments and product of inertia
j	$=\sqrt{-1}$
L, N, Y	gust-induced rolling moment, yawing moment, and side force, respectively
L'	integral scale of turbulence
L_p	$=\rho U_o S b^2 C_{\ell_p} / 4I_x$
L_r	$=\rho U_o S b^2 C_{\ell_r} / 4I_x$
L_v	$=\rho U_o S b\, C_{\ell\beta} / 2I_x$
$\ell(u_g)$	wing lift due to u_g
$\ell(w_g)$	wing lift due to w_g
M	airplane mass
N_p	$=\rho U_o S b^2 C_{n_p} / 4I_z$
N_r	$=\rho U_o S b^2 C_{n_r} / 4I_z$

NOMENCLATURE (Continued)

N_v	$= \rho U_o S b C_{n\beta} / 2 I_z$
$N_{\dot{v}}$	$= \rho U_o S b C_{n\dot{\beta}} / 2 I_z$
p, r	rolling and yawing velocities
S	planform reference area
s	Laplace transform complex variable
U, V, W	orthogonal components of total relative wind velocity
u_g, v_g, w_g	orthogonal gust velocity components
Y_p	$= \rho U_o S b C_{y_p} / 4 M$
Y_r	$= \rho U_o S b C_{y_r} / 4 M$
Y_v	$= \rho U_o S C_{y\beta} / 2 M$
α, β, θ	perturbation angles of attack, sideslip, and pitch
α_o	steady state or trim angle of attack
β_g	gust-induced sideslip angle
γ_o	trim flight path angle
ρ	free stream air density
$\sigma_{u_g}, \sigma_{v_g}, \sigma_{w_g}$	rms values of gust velocity components
$\sigma_\beta, \sigma_\psi, \sigma_\phi$	rms values of sideslip, yaw, and roll response angles
$\Phi_{D\phi_g}, \Phi_{D\psi_g}$	power spectral densities of equivalent rolling and yawing gust gradients
$\Phi_{L(w_g)}, \Phi_{N(w_g)}$	power spectral densities of w_g - induced rolling and yawing moments
$\Phi_{L(u_g)}, \Phi_{N(u_g)}$	power spectral densities of u_g - induced rolling and yawing moments
$\Phi_{Y(v_g)}$	power spectral density of v_g - induced side force
$\Phi_{u_g}, \Phi_{v_g}, \Phi_{w_g}$	power spectral densities of gust velocity components

NOMENCLATURE (Continued)

Φ_β ,Φ_ψ ,Φ_ϕ	power spectral densities of sideslip, yaw, and roll response angles
ϕ , ψ	perturbation roll and yaw response angles

Subscripts

W	wing effects
T	vertical tail effects
WT	wing and vertical tail effects
FT	fuselage and vertical tail effects
o	steady state, mean, or trim value
g	gust effects

SECTION I

INTRODUCTION

The design of flight control systems for VTOL aircraft is still very much an art rather than a well-defined and documented procedure. Attempts to apply to VTOL design the analytical approaches which were developed for conventional types of aircraft have had only limited success. One such area of limited success is in analytically modeling and analyzing the dynamic response to atmospheric turbulence during hover and transition flight. A fundamental difficulty in this case involves providing a valid analytical representation of the turbulence-generated disturbance forces and moments acting on the aircraft.

Major sources of aerodynamic forces and moments acting on VTOL aircraft in low-altitude hover or near-hover flight modes are the three orthogonal components of wind relative velocity U, V, and W where, in general, each contains a mean or steady relative wind component U_o, V_o, and W_o, and turbulence or gust components u_g, v_g, and w_g. For purposes of point stability or frozen point dynamic analysis, the aircraft is usually assumed headed into the mean wind. In this case,

$$U = U_o + u_g \quad ; \quad V = v_g \quad ; \quad W = w_g$$

u_g, v_g, and w_g will create forces and moments on the aircraft primarily by two mechanisms:

(1) Circulation lift due to Bernoulli's theorem and the Kutta-Joukowsky law of circulation;

(2) Momentum transfer between the gust velocity components and the airframe.

For conventional aircraft, where the flight speed is essentially U_o and $U_o >> u_g, v_g, w_g, V_o, W_o$, the gust aerodynamic forces and moments (other than drag) are largely due to circulation lift. However, as a VTOL aircraft transitions to hovering flight, the contribution due to circulation decreases to the point where it may well be of the same order of magnitude as the contribution due to momentum transfer when turbulence is severe. Therefore, a valid aerodynamic theory in the hovering mode must account for both types of inputs.

Circulation lift theories are well developed for conventional aircraft and express the results in Taylor series expansions (based on small perturbations) involving coefficients and stability derivatives. Such theories are not nearly as accurate for VTOL hover due to violation of the small angle assumption on gust inputs--that is, inputs in the nonlinear range of the lift curve slope. There are no good aerodynamic theories which adequately describe the gust input forces and moments due to either circulation or momentum transfer, let alone both simultaneously, for VTOL vehicles in or near hover. Consequently, VTOL designers continue to use the stability derivative approach for describing vehicle gust input forces in hover even though the applicability is questionable in many cases. It should be pointed out, however, that it is still probably accurate enough to use a Taylor series expansion (with stability derivatives) of the aerodynamic forces and moments resulting from the motions of the aircraft. These motions are likely to be within the small perturbation assumption on the dependent variables such as pitch angle, θ, and angle of attack, α, particularly where the VTOL vehicle has a stability augmentation system (as most do) which tends to maintain small angle responses to gusts and other disturbances.

A further complication in computing the gust forces and moments occurs when one wishes to account for the effects of distributed gust velocities along the fuselage (penetration effects)

and across the wing span. For example, variations in longitudinal component, u_g, and vertical component, w_g, across the wing span at any time instant will induce rolling and yawing moments, as will variations in lateral component, v_g, along the fuselage. This is illustrated in Figure 1. The objective of the research reported herein was to determine the importance of these gust velocity distributions on determination of the lateral-directional response of hovering VTOL aircraft.

The approach taken, using power spectral density analytical techniques, was to compare the vehicle yaw, roll, and sideslip angle responses with and without the velocity distribution effects. The critical factor was the mathematical method used to describe the gust input forces and moments. To the authors' knowledge, only two methods are available and both were developed for application to aircraft in conventional flight where the flight velocity is much larger than the gust component velocities. This assures that the gust-induced forces and moments are due largely to circulation lift, with negligible momentum transfer between gust field and aircraft. The first method (Reference 1) uses aerodynamic transfer functions to describe the gust input forces and moments. This method requires considerably more information on the aerodynamic characteristics of the aircraft in the form of frequency response functions than the second. For this reason the second method (Reference 2) was used to describe the gust-induced forces and moments acting on the hovering aircraft. In this method the gust velocities are represented as equivalent rigid-body rotations of the airplane; namely, rolling, yawing, and side gusts. The random distributions of gust velocities across the span, and the fuselage penetration effects are accounted for in defining the rolling, yawing, and side gusts. Flow field interaction effects due to lift intake and engine exhaust were neglected, though they would be important in a quantitative design.

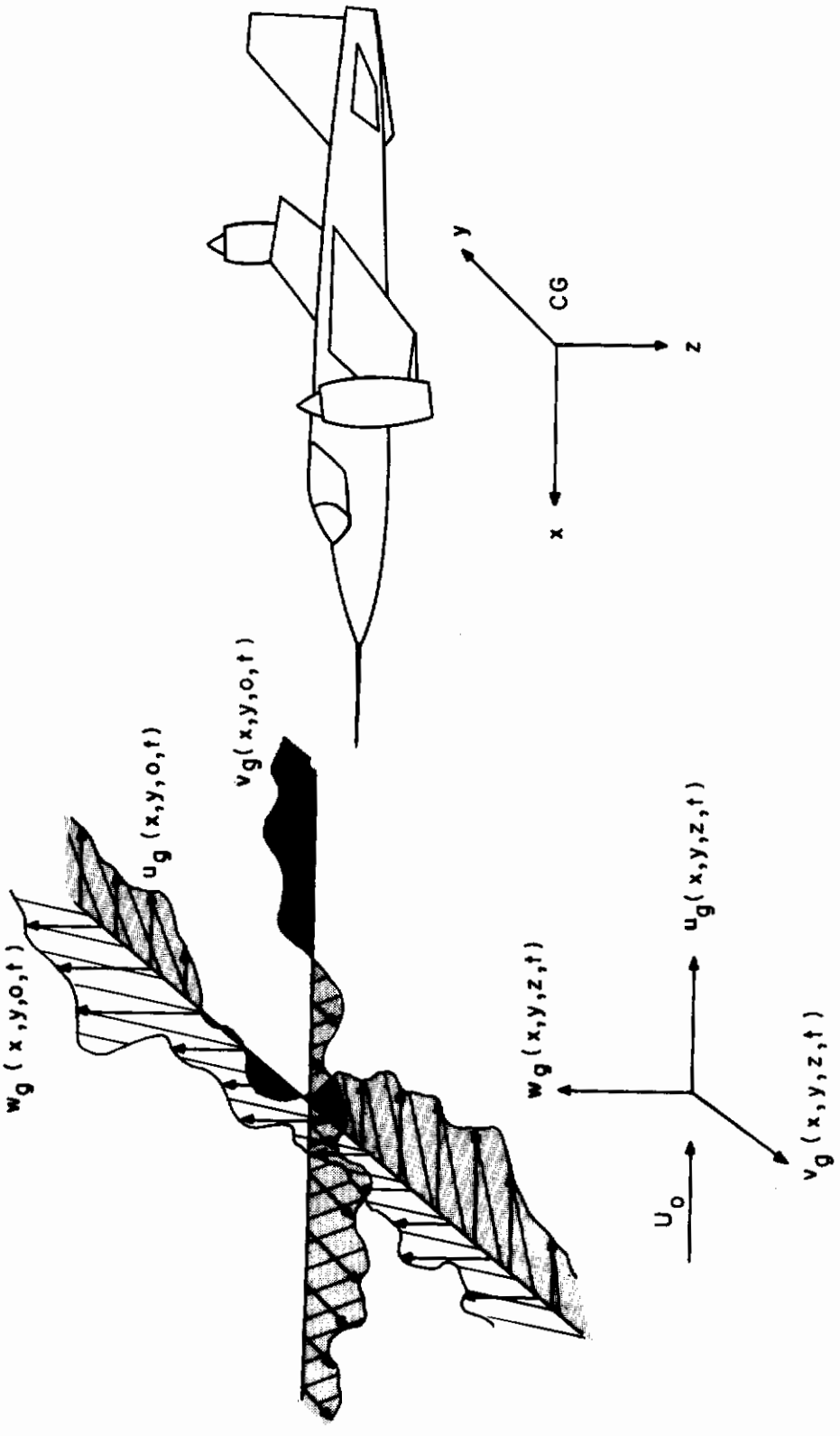

Figure 1. Gust Spatial Distributions

SECTION II

EQUATIONS OF MOTION

The three-degree-of-freedom lateral-directional, small-perturbation equations of motion of a free airframe can be written as in Equation (1) (see Reference 3):

$$\begin{bmatrix} MU_o\,(s - Y_v) & -MY_r\,s - M_g \sin\gamma_o & M(-Y_p\,s - g\cos\gamma_o) \\ -I_z U_o\,(N_{\dot{v}}\,s + N_v) & I_z\,(s^2 - N_r\,s) & -I_{xz}\,s^2 - I_z N_p\,s \\ -I_x U_o L_v & -I_{xz}\,s^2 - I_x L_r\,s & I_x\,(s^2 - L_p\,s) \end{bmatrix} \begin{bmatrix} \beta \\ \psi \\ \phi \end{bmatrix} = \begin{bmatrix} Y \\ N \\ L \end{bmatrix} \qquad (1)$$

β, ψ, and ϕ are the small perturbation sideslip, yaw, and roll angles, respectively. Y, N, and L are the respective side force, yawing moment, and rolling moment induced by the three components of gust velocity, u_g, v_g, and w_g.

To simplify the description of Y, N, and L, it has been assumed that the side force, Y, is due to v_g acting on the fuselage and vertical tail, the yawing moment, N, is due to u_g and w_g acting on the wing and v_g acting on the fuselage and vertical tail, and the rolling moment, L, is due to u_g, v_g, and w_g acting on the wing and v_g acting on the vertical tail. Thus,

$$Y = Y_{FT}(v_g)$$

$$N = N_W(u_g, w_g) + N_{FT}(v_g)$$

$$L = L_W(u_g, v_g, w_g) + L_T(v_g)$$

or, linearized and in matrix transfer function form,

$$\begin{bmatrix} Y \\ N \\ L \end{bmatrix} = \begin{bmatrix} 0 & \left(\frac{Y}{v_g}\right)_{FT} & 0 \\ \left(\frac{N}{u_g}\right)_W & \left(\frac{N}{v_g}\right)_{FT} & \left(\frac{N}{w_g}\right)_W \\ \left(\frac{L}{u_g}\right)_W & \left\{\left(\frac{L}{v_g}\right)_W + \left(\frac{L}{v_g}\right)_T\right\} & \left(\frac{L}{w_g}\right)_W \end{bmatrix} \begin{bmatrix} u_g \\ v_g \\ w_g \end{bmatrix} \qquad (2)$$

Denoting the square matrix in Equation (1) by D(s), we have

$$\begin{bmatrix} \beta \\ \psi \\ \phi \end{bmatrix} = \left[D(S)\right]^{-1} \begin{bmatrix} Y \\ N \\ L \end{bmatrix} = \begin{bmatrix} \left(\frac{\beta}{Y}\right) & \left(\frac{\beta}{N}\right) & \left(\frac{\beta}{L}\right) \\ \left(\frac{\psi}{Y}\right) & \left(\frac{\psi}{N}\right) & \left(\frac{\psi}{L}\right) \\ \left(\frac{\phi}{Y}\right) & \left(\frac{\phi}{N}\right) & \left(\frac{\phi}{L}\right) \end{bmatrix} \begin{bmatrix} Y \\ N \\ L \end{bmatrix} \qquad (3)$$

Combining Equations (2) and (3) gives the matrix equation (4).

$$\begin{bmatrix} \beta \\ \psi \\ \phi \end{bmatrix} = \begin{bmatrix} \left\{\left(\frac{\beta}{N}\right)\left(\frac{N}{u_g}\right)_W + \left(\frac{\beta}{L}\right)\left(\frac{L}{u_g}\right)_W\right\} & \left\{\left(\frac{\beta}{Y}\right)\left(\frac{Y}{v_g}\right)_{FT} + \left(\frac{\beta}{N}\right)\left(\frac{N}{v_g}\right)_{FT}\right. \\ \left\{\left(\frac{\psi}{N}\right)\left(\frac{N}{u_g}\right)_W + \left(\frac{\psi}{L}\right)\left(\frac{L}{u_g}\right)_W\right\} & \left\{\left(\frac{\psi}{Y}\right)\left(\frac{Y}{v_g}\right)_{FT} + \left(\frac{\psi}{N}\right)\left(\frac{N}{v_g}\right)_{FT}\right. \\ \left\{\left(\frac{\phi}{N}\right)\left(\frac{N}{u_g}\right)_W + \left(\frac{\phi}{L}\right)\left(\frac{L}{u_g}\right)_W\right\} & \left\{\left(\frac{\phi}{Y}\right)\left(\frac{Y}{v_g}\right)_{FT} + \left(\frac{\phi}{N}\right)\left(\frac{N}{v_g}\right)_{FT}\right. \end{bmatrix}$$

$$\begin{bmatrix} + \left(\frac{\beta}{L}\right)\left[\left(\frac{L}{v_g}\right)_W + \left(\frac{L}{v_g}\right)_T\right]\right\} & \left\{\left(\frac{\beta}{N}\right)\left(\frac{N}{w_g}\right)_W + \left(\frac{\beta}{L}\right)\left(\frac{L}{w_g}\right)_W\right\} \\ + \left(\frac{\psi}{L}\right)\left[\left(\frac{L}{v_g}\right)_W + \left(\frac{L}{v_g}\right)_T\right]\right\} & \left\{\left(\frac{\psi}{N}\right)\left(\frac{N}{w_g}\right)_W + \left(\frac{\psi}{L}\right)\left(\frac{L}{w_g}\right)_W\right\} \\ + \left(\frac{\phi}{L}\right)\left[\left(\frac{L}{v_g}\right)_W + \left(\frac{L}{v_g}\right)_T\right]\right\} & \left\{\left(\frac{\phi}{N}\right)\left(\frac{N}{w_g}\right)_W + \left(\frac{\phi}{L}\right)\left(\frac{L}{w_g}\right)_W\right\} \end{bmatrix} \begin{bmatrix} u_g \\ v_g \\ w_g \end{bmatrix} = [a_{ij}] \begin{bmatrix} u_g \\ v_g \\ w_g \end{bmatrix} \quad (4)$$

In terms of power spectral densities and assuming u_g, v_g, and w_g are uncorrelated, we have

$$\Phi_\beta(\omega) = |a_{11}(\omega)|^2 \Phi_{u_g}(\omega) + |a_{12}(\omega)|^2 \Phi_{v_g}(\omega) + |a_{13}(\omega)|^2 \Phi_{w_g}(\omega) \quad (5)$$

$$\Phi_\psi(\omega) = |a_{21}(\omega)|^2 \Phi_{u_g}(\omega) + |a_{22}(\omega)|^2 \Phi_{v_g}(\omega) + |a_{23}(\omega)|^2 \Phi_{w_g}(\omega) \quad (6)$$

$$\Phi_\phi(\omega) = |a_{31}(\omega)|^2 \Phi_{u_g}(\omega) + |a_{32}(\omega)|^2 \Phi_{v_g}(\omega) + |a_{33}(\omega)|^2 \Phi_{w_g}(\omega) \quad (7)$$

The infinite integrals of Equations (5), (6), and (7) yield the variances or mean square values of the aircraft response angles, β, ψ, and ϕ.

$$\sigma_\beta^2 = \int_{-\infty}^{\infty} \Phi_\beta(\omega)\, d\omega \quad (8)$$

$$\sigma_\psi^2 = \int_{-\infty}^{\infty} \Phi_\psi(\omega)\, d\omega \quad (9)$$

$$\sigma_\phi^2 \int_{-\infty}^{\infty} \Phi_\phi(\omega)\, d\omega \quad (10)$$

To assess the importance of spanwise and longitudinal (penetration) distributions of gust velocities on hovering VTOL aircraft, Equations (8), (9), and (10) were evaluated for a hovering VJ-101 (Figure 2) both with and without distribution effects. From this analysis of a single configuration it was possible to draw some general conclusions.

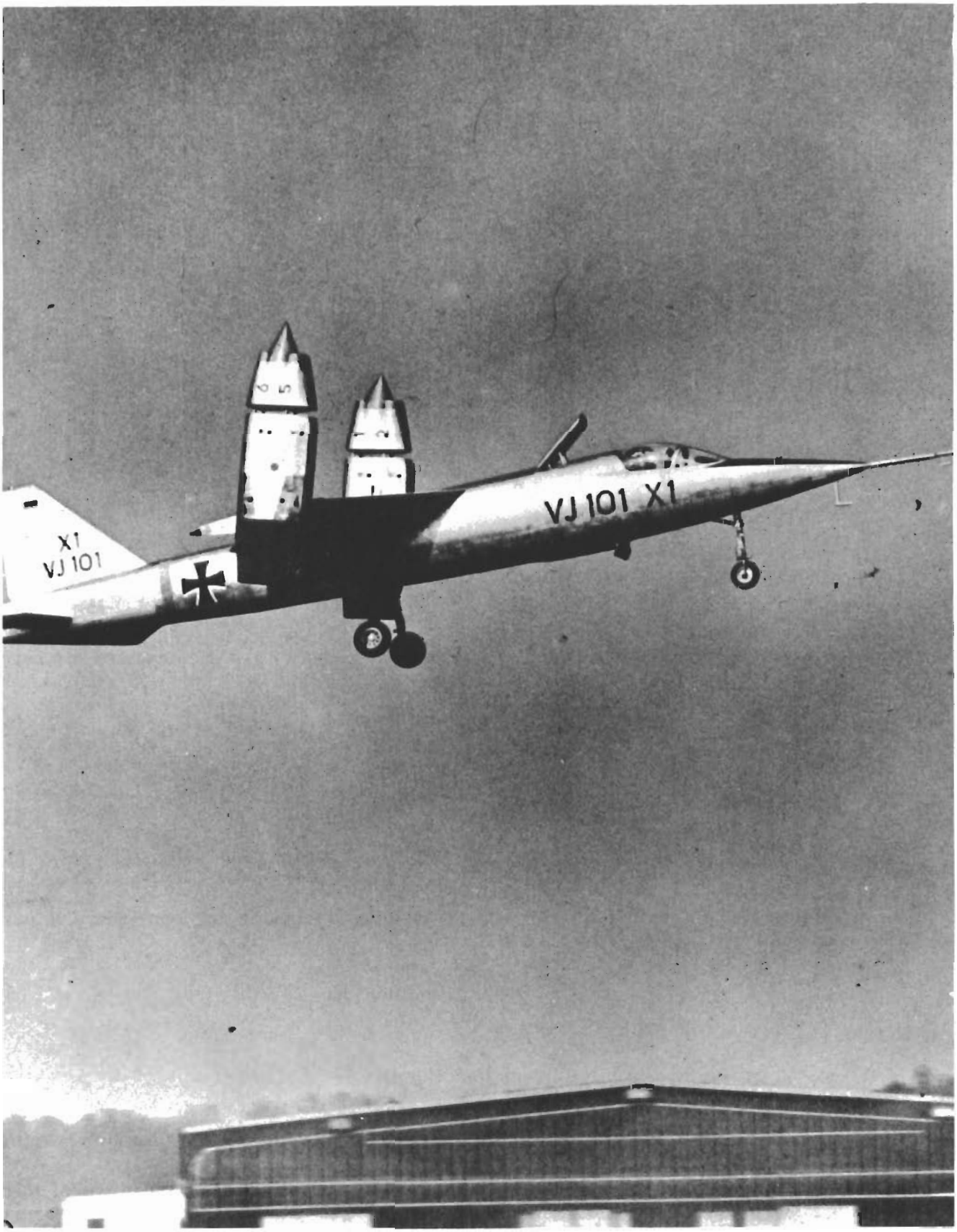

Figure 2. VJ-101 In Hover

The a_{ij} matrix in Equation (4) relates the response angles to the component gust velocities. The elements of a_{ij}, as a function of frequency, are dependent on the airframe transfer functions of Equation (3) and the gust input transfer functions of Equation (2). The distribution effects are included in the gust transfer functions.

The flight condition analyzed was that of near-hover (over a spot) at 50 ft altitude and headed into a 25 ft/sec mean wind. The data used in evaluating the elements of Equation (1) are:

U_o = 25 ft/sec; γ_o = 5.5 deg; g = 32.2 ft/sec^2; M = 471.8 slugs;

I_x = 18,530 slug-ft^2; I_z = 45,700 slug-ft^2; I_{xz} = 5200 slug-ft^2;

Y_v = -0.034; α_o = -7.5 deg; L_v = -0.00384; N_v 0.000863; N_v = 0;

Y_r = 0.106; L_r = 0.0109; N_r = -0.0228; Y_p = -0.0182; L_p = -0.0131;

N_p = -.00268.

With the substitution of $s = j\omega$, the nine airframe transfer functions of Equation (3) were determined as a function of ω from Equation (1). The denominator for each of these nine is

$$\Delta(s) = s(s + 0.0213)(s + 0.507)(s^2 - 0.458s + 0.233) \tag{11}$$

The negative damping in the quadratic factor indicates the vehicle is unstable and would require stabilization by a stability augmentation system and/or a pilot in the control loop. Without getting into a discussion of what constitutes desirable handling qualities, it was assumed augmentation could be provided which would yield the following closed-loop characteristic polynomial:

$$\bar{\Delta}(s) = (s + 0.1)(s + 0.2)(s + 0.3)(s^2 + 0.2s + 1) \tag{12}$$

In Equation (12) the dutch-roll quadratic has a damping ratio of 0.1 and natural frequency of 1.0 rad/sec. In the frequency domain,

$$\frac{\Delta(\omega)}{\bar{\Delta}(\omega)} = \frac{(0.0705\omega^4 - 0.117\omega^2) + j(\omega^5 - 0.0014\omega^3 + 0.0025\omega)}{(0.8\omega^4 - 0.628\omega^2 + 0.006) + j(\omega^5 - 1.23\omega^3 + 0.1112\omega)} \tag{13}$$

The products of Equation (13) and each of the airframe transfer functions of Equation (3) give the closed-loop airframe transfer functions. These are used in the evaluation of the a_{ij} matrix of Equation (4).

SECTION III

GUST-INDUCED FORCES AND MOMENTS

Following the method in References 2 and 4 of representing the gust velocities as equivalent rigid-body rotations, consider

$$L(w_g) = -\frac{1}{2}\rho U_o^2 Sb(C_{\ell_p})_W \frac{p_g b}{2U_o} = \frac{1}{4}\rho U_o^2 Sb(C_{\ell_p})_W D\phi_g \quad (14)$$

$$L(u_g) = -\frac{1}{2}\rho U_o^2 Sb(C_{\ell_r})_W \frac{r_g b}{2U_o} = \frac{1}{4}\rho U_o^2 Sb(C_{\ell_r})_W D\psi_g \quad (15)$$

At any instant, the random distribution of vertical gust velocity w_g across the span has some equivalent average linear spanwise gradient which produces the wing rolling moment $L(w_g)$. $D\phi_g$ as defined by Equation (14) is that equivalent rolling gust gradient. Likewise, $D\psi_g$ is the equivalent yawing gust gradient due to spanwise distribution of u_g. w_g also produces a wing yawing moment which is assumed to be in phase with the rolling moment (see Reference 4 for justification). Likewise, u_g produces a wing yawing moment. Thus,

$$N(w_g) = \left(\frac{C_{n_p}}{C_{\ell_p}}\right)_W L(w_g) = \frac{1}{4}\rho U_o^2 Sb(C_{n_p})_W D\phi_g \quad (16)$$

$$N(u_g) = \left(\frac{C_{n_r}}{C_{\ell_r}}\right)_W L(u_g) = \frac{1}{4}\rho U_o^2 Sb(C_{n_r})_W D\psi_g \quad (17)$$

The turbulence is assumed to be homogeneous and isotropic. The statistical properties of the gust patches are also assumed constant as they traverse the aircraft (Taylor's hypothesis). u_g, v_g, and w_g are assumed to have the following power spectral densities:

$$\Phi_{u_g} = \frac{\sigma_{u_g}^2 L'}{\pi U_o} \cdot \frac{1}{1+\left(\frac{\omega L'}{U_o}\right)^2} \quad (18)$$

$$\Phi_{v_g} = U_o^2 \Phi_{\beta_g} = \Phi_{w_g} = \frac{\sigma_{v_g}^2 L'}{2\pi U_o} \cdot \frac{1+3\left(\frac{\omega L'}{U_o}\right)^2}{\left[1+\left(\frac{\omega L'}{U_o}\right)^2\right]^2} \quad (19)$$

where

$$\sigma_{u_g}^2 = \sigma_{v_g}^2 = \sigma_{w_g}^2$$

and

$$\sigma_{u_g}^2 = \int_{-\infty}^{\infty} \Phi_{u_g} d\omega = \int_{-\infty}^{\infty} \Phi_{v_g} d\omega = \int_{-\infty}^{\infty} \Phi_{w_g} d\omega$$

There is room for argument as to whether or not this mathematical model accurately represents low-altitude turbulence — particularly since such turbulence is not strictly isotropic; however, the model is sufficiently accurate for our purposes here.

Now,

$$\Phi_{D\phi_g} = \left|\frac{D\phi_g}{\beta_g}\right|^2 \Phi_{\beta_g} = \left|\frac{D\phi_g}{\beta_g}\right|^2 \frac{\Phi_{w_g}}{U_o^2} \tag{20}$$

and

$$\Phi_{D\psi_g} = \left|\frac{D\psi_g}{\beta_g}\right|^2 \Phi_{\beta_g} = \left|\frac{D\psi_g}{\beta_g}\right|^2 \frac{\Phi_{w_g}}{U_o^2} \tag{21}$$

Thus, from Equations (14) and (15),

$$\Phi_{L(w_g)} = \frac{\left[\frac{1}{4}\rho U_o^2 S b (C_{\ell_p})_W\right]^2}{U_o^2} \left|\frac{D\phi_g}{\beta_g}\right|^2 \Phi_{w_g} \tag{22}$$

$$\Phi_{L(u_g)} = \frac{\left[\frac{1}{4}\rho U_o^2 S b (C_{\ell_p})_W\right]^2}{U_o^2} \left|\frac{D\psi_g}{\beta_g}\right|^2 \Phi_{w_g} \tag{23}$$

And from Equations (16) and (17),

$$\Phi_{N(w_g)} = \left(\frac{C_{n_p}}{C_{\ell_p}}\right)_W^2 \Phi_{L(w_g)} \tag{24}$$

$$\Phi_{N(u_g)} = \left(\frac{C_{n_r}}{C_{\ell_r}}\right)_W^2 \Phi_{L(u_g)} \tag{25}$$

$\left|\frac{D\phi_g}{\beta_g}\right|^2$ and $\left|\frac{D\psi_g}{\beta_g}\right|^2$ are obtained from Figures 15 and 16 of Reference 2, which are reproduced here as Figures 3 and 4. The details of the derivations of these curves are given in Reference 2 and 4 and will not be repeated here. A few words concerning the assumptions made are in order, however. The theory used assumes that the aerodynamic forces vary linearly with u_g and w_g. This implies that u_g and w_g must be sufficiently small compared to the mean wind U_o. The lift curve slopes of most subsonic wings are linear up to about 14 degrees angle of attack. Therefore, since the gust-induced angle of attack is given by $\alpha_g = \arctan\frac{w_g}{U_o} \cong \frac{w_g}{U_o}$, for a mean wind of 25 ft/sec, we must have $w_g \leq 6$ ft/sec, approximately for low trim angles of attack. For gust velocities larger than this, the assumption of linear aerodynamics is less valid and momentum transfer of gust energy to the aircraft becomes significant compared to forces due to circulation lift. A further assumption of the linear theory on which Figures 3 and 4 are based is that the ratio of wing lift due to u_g and wing lift due to w_g is given by (see Reference 4)

$$\frac{\ell(u_g)}{\ell(w_g)} = 2\alpha_o \frac{u_g}{w_g} \tag{26}$$

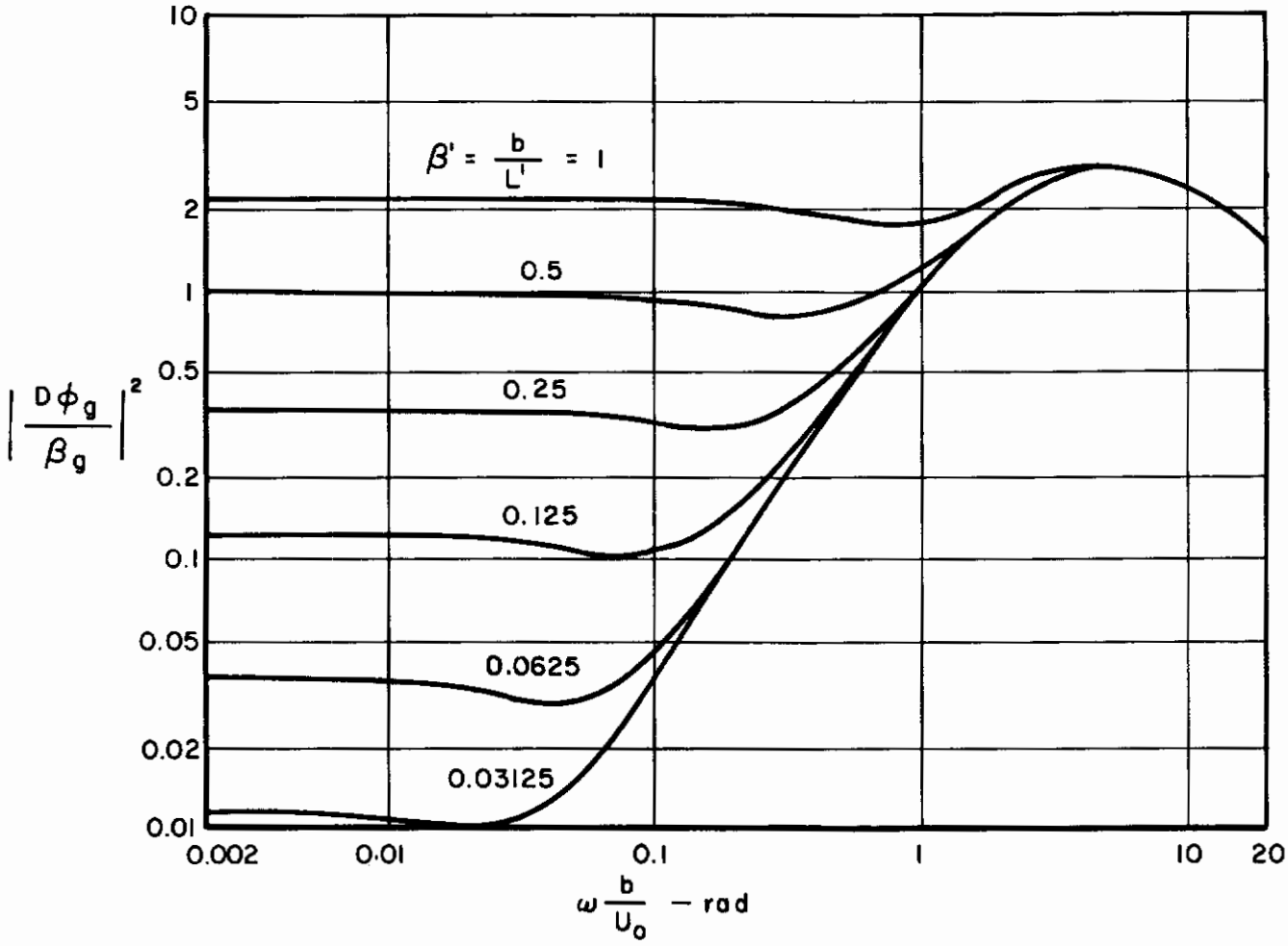

Figure 3. Ratio of Rolling Gust to Side Gust Spectra (Reference 2)

We have

$$\ell(u_g) = \frac{1}{2}\rho\left[(U_o + u_g)^2 - U^2\right] SC_{L_\alpha}\ \alpha_o \tag{27}$$

$$\ell(w_g) = \frac{1}{2}\rho\, U_o^2\, SC_{L_\alpha}\left(\arctan\frac{w_g}{U_o}\right) \tag{28}$$

$$\frac{\ell(u_g)}{\ell(w_g)} = \frac{(u_g^2 + 2U_o u_g)\alpha_o}{U_o^2\ \arctan\frac{w_g}{U_o}} \tag{29}$$

Comparison of Equations (26) and (29) shows they are nearly equal if $u_g << U_o$ and $w_g << U_o$. If $u_g = w_g = 6$ ft/sec, then Equation (29) gives $\ell(u_g)/\ell(w_g) = 2.24\ \alpha_o$, compared to $2\alpha_o$ from Equation (26) — about a 10% error. With the limit of about 6 ft/sec on u_g and w_g magnitudes, the aerodynamic theory used is reasonably accurate in accounting for the gust forces acting on the aircraft hovering in a 25 ft/sec mean wind at low angles of attack. And in fact reasonably good representation can be expected as long as the ratios of component gust velocities to mean wind velocity are less than about 6/25.

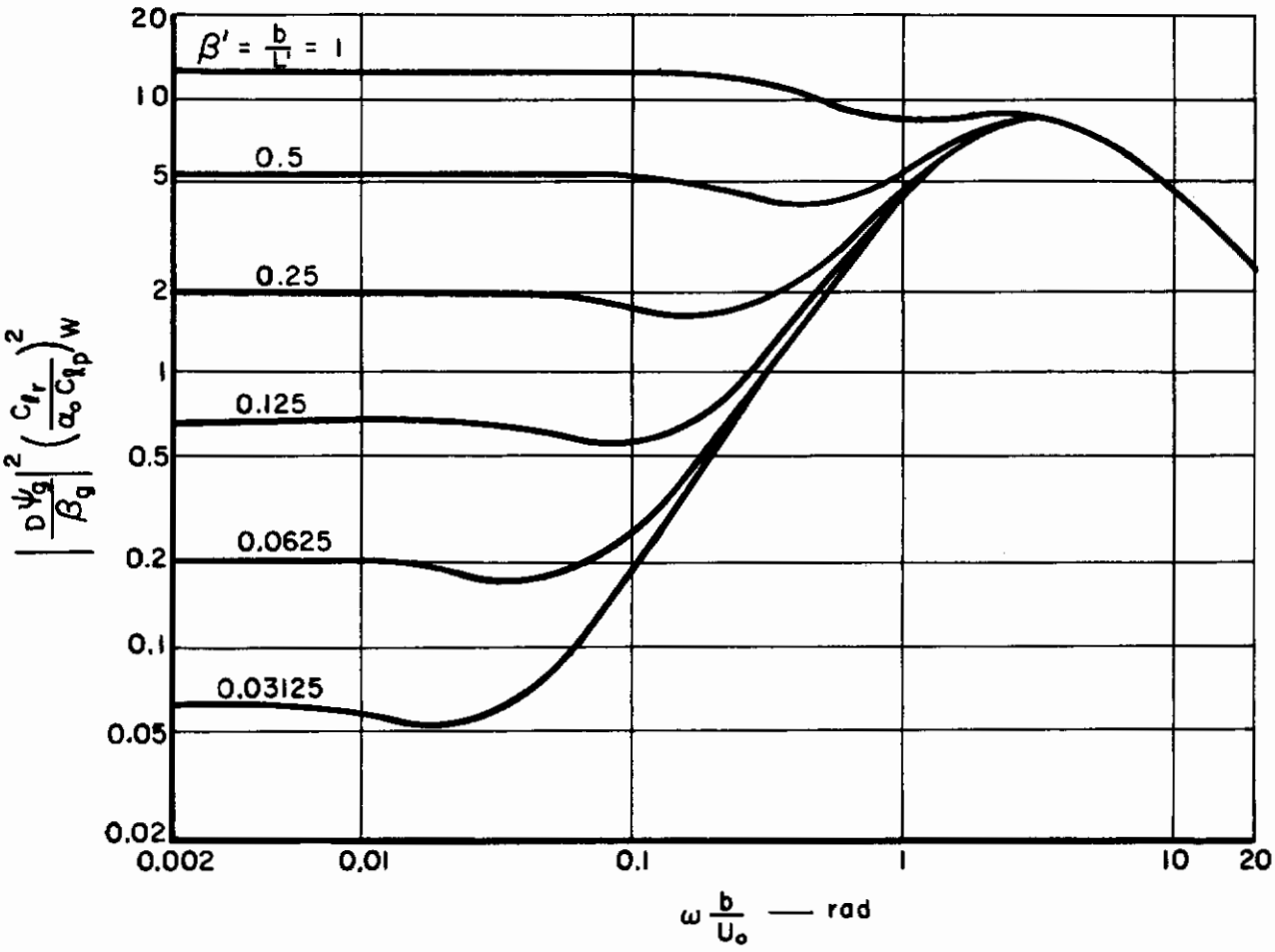

Figure 4. Ratio of Yawing Gust to Side Gust Spectra (Reference 2)

Consider now the effects of the lateral gust velocity component v_g. The yawing moment of the fuselage and vertical tail, due to penetration into lateral gusts referenced at the center of gravity, has been derived in Reference 5 where a simple profile shape was used to define the side force distribution over the fuselage and vertical tail due to sinusoidal v_g components. As developed in Reference 5 and summarized in Reference 2,

$$\left(\frac{N}{v_g}\right)_{FT} = \pi\rho U_o \left\{ \frac{-2x_o s_o^2}{k_o^3}\left[(2k_o - jk_o^2 + j2)e^{jk_o} - j2\right] \right.$$

$$\left. + \frac{(x_2-x_1)(s_1-s_o)^2}{(k_2-k_1)^3}\left[(2k_2 - k_1 - j2 - jk_1k_2 + jk_2^2)e^{-jk_2} - (k_1 - j2)e^{-jk_1}\right]\right\} \qquad (30)$$

where $k_n = \frac{\omega x_n}{U_o}$ (n=0, 1, 2); and x_o, x_1, x_2, s_o, and s_1 are the profile dimensions shown in Figure 5. Equation (30) is based on slender-body theory and requires small sideslip angles—again $\frac{v_g}{U_o} \leq \frac{6}{25}$ gives about 10% error. The side force transfer function is given in Equation (31).

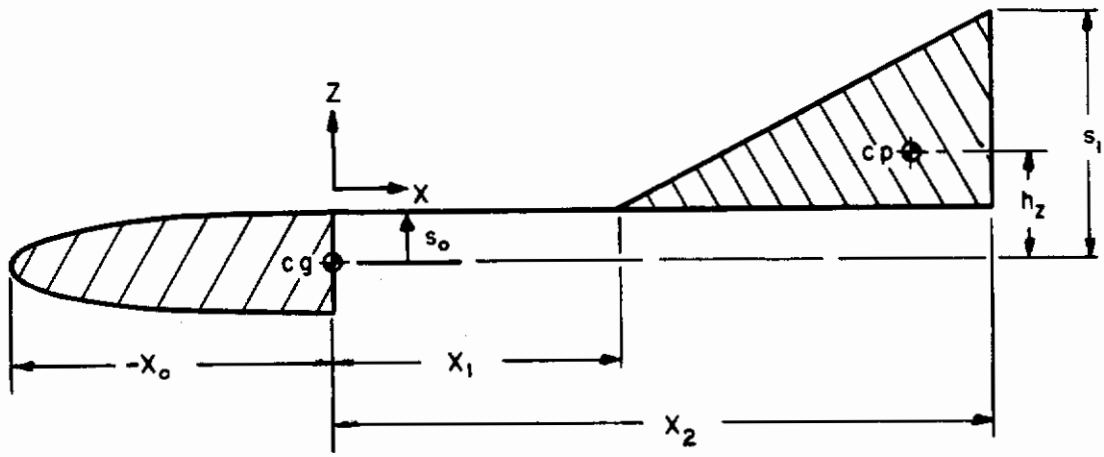

Figure 5. Fuselage Profile

$$\left(\frac{Y}{v_g}\right)_{FT} = \pi\rho U_o \left\{\frac{2s_o^2}{k_o^2}\left[1-(1-jk_o)e^{jk_o}\right] + \left(\frac{s_1-s_o}{k_2-k_1}\right)^2\left[e^{-jk_1}-(1-jk_1+jk_2)e^{-jk_2}\right]\right\} \quad (31)$$

Now, at $\omega = 0$ it can be shown that Equations (30) and (31) reduce to

$$\left(\frac{N}{v_g}\right)_{FT} = \frac{\pi\rho U_o}{3}\left[-2s_o^2 x_o + (s_1-s_o)^2\left(x_2+\frac{x_1}{2}\right)\right] = \frac{1}{2}\rho U_o S b (C_{n_\beta})_{FT} \quad (32)$$

$$\left(\frac{Y}{v_g}\right)_{FT} = \frac{-\pi\rho U_o}{2}\left[2s_o^2 + (s_1-s_o)^2\right] = \frac{1}{2}\rho U_o S (C_{y_\beta})_{FT} \quad (33)$$

$(C_{n_\beta})_{FT}$ and $(C_{y_\beta})_{FT}$ are fuselage-tail steady-state stability derivatives, and the profile parameters in Figure 5 should be adjusted so that Equations (32) and (33) are satisfied. These profile dimensions are not physical dimensions on the vehicle but are selected to match the above theory to the steady-state stability derivatives of the vehicle.

The rolling moment transfer function due to lateral gusts on the wing and vertical tail is

$$\left(\frac{L}{v_g}\right)_{WT} = \left(\frac{L}{v_g}\right)_W + \left(\frac{L}{v_g}\right)_T \quad (34)$$

where

$$\left(\frac{L}{v_g}\right)_W = \frac{1}{2}\rho U_o S b (C_{l_\beta})_W \quad (35)$$

As derived in Reference 5, the second term in Equation (31) is the side force due to the vertical tail. Thus,

$$\left(\frac{L}{v_g}\right)_T = \pi \rho U_o h_z \left(\frac{s_1 - s_o}{k_2 - k_1}\right)^2 \left[e^{-jk_1} - (1 - jk_1 + jk_2)\, e^{-jk_2}\right] \tag{36}$$

where h_z is the distance of the vertical tail profile center of pressure above the x-axis. At $\omega = 0$, it can be shown that Equation (36) reduces to

$$\left(\frac{L}{v_g}\right)_T = -\frac{1}{2}\, \pi \rho U_o h_z (s_1 - s_o)^2 = \frac{1}{2} \rho U_o Sb (C_{\ell\beta})_T \tag{37}$$

where $(C_{\ell_\beta})_T$ is the vertical tail rolling moment due to sideslip steady-state stability derivative. h_z must be chosen so that Equation (37) is satisfied. Thus,

$$h_z = \frac{-Sb (C_{\ell\beta})_T}{\pi (s_1 - s_o)^2} \tag{38}$$

Combining Equations (34), (35), (36), and (38) gives

$$\left(\frac{L}{v_g}\right)_{WT} = \left(\frac{L}{v_g}\right)_W + \left(\frac{L}{v_g}\right)_T$$

$$= \frac{-\rho U_o Sb (C_{\ell\beta})_T}{(k_2 - k_1)^2} \left[e^{-jk_1} - (1 - jk_1 + jk_2)\, e^{-jk_2}\right] + \frac{1}{2} \rho U_o Sb (C_{\ell\beta})_W \tag{39}$$

For the VJ-101 aircraft and flight condition analyzed herein, the steady-state stability derivatives and profile parameters needed in the above equations are tabulated below.

$(C_{\ell\beta})_W = -0.3$	$(C_{y\beta})_{FT} = -2.711$	$x_1 = -18$ ft
$(C_{\ell\beta})_T = -0.307$	$(C_{n\beta})_{FT} = 0.337$	$x_2 = 16$ ft
$(C_{\ell r})_W = 0.175$	$b = 19.69$ ft	$k_o = 0.96\,\omega$ rad
$(C_{\ell p})_W = -0.21$	$S = 200$ ft^2	$k_1 = -0.72\,\omega$ rad
$(C_{y\beta})_T = -2.43$	$s_o = 3$ ft	$k_2 = 0.64\,\omega$ rad
$(C_{n_r})_W = -0.1$	$s_1 = 15.45$ ft	
$(C_{n_p})_W = -0.106$	$x_o = 24$ ft	

The power spectral densities of yawing moment, rolling moment, and side force due to v_g are given by

$$\Phi_{N(v_g)} = \left|\left(\frac{N}{v_g}\right)_{FT}\right|^2 \Phi_{v_g} \tag{40}$$

$$\Phi_{L(v_g)} = \left|\left(\frac{L}{v_g}\right)_{WT}\right|^2 \Phi_{v_g} \tag{41}$$

$$\Phi_{Y(v_g)} = \left|\left(\frac{Y}{v_g}\right)_{FT}\right|^2 \Phi_{v_g} \tag{42}$$

Equations (40), (41), and (42) were evaluated for discrete values of frequency ω and are shown plotted in Figures 6, 7, and 8. The curves are normalized by the mean square values of gust velocity as given in the turbulence models of Equations (18) and (19). Likewise, Equations (22), (23), (24), and (25) were evaluated and plotted on the same figures.

The dashed curves on Figures 6, 7, and 8 are the power spectra of gust-induced yawing moment, rolling moment, and side force with uniform spanwise and axial distribution of gust velocities. Uniform u_g and w_g across the span will produce no yawing or rolling moments, and v_g uniform axially means lateral gust penetration effects are not included. With uniform distributions, in terms of total aircraft derivatives,

$$Y = \frac{1}{2} \rho U_o S C_{y_\beta} v_g \tag{43}$$

$$N = \frac{1}{2} \rho U_o Sb C_{n_\beta} v_g \tag{44}$$

$$L = \frac{1}{2} \rho U_o Sb C_{\ell_\beta} v_g \tag{45}$$

And the power spectra are

$$\Phi_{Y(v_g)} = \left|\frac{1}{2} \rho U_o S C_{y_\beta}\right|^2 \Phi_{v_g} \tag{46}$$

$$\Phi_{N(v_g)} = \left|\frac{1}{2} \rho U_o Sb C_{n_\beta}\right|^2 \Phi_{v_g} \tag{47}$$

$$\Phi_{L(v_g)} = \left|\frac{1}{2} \rho U_o Sb C_{\ell_\beta}\right|^2 \Phi_{v_g} \tag{48}$$

Examination of Figure 6 shows that yawing moment due to u_g is an order of magnitude less than that due to w_g which is, in turn, two to three orders of magnitude less than that due to v_g. Comparison of the two $\Phi_{N(v_g)}$ spectra shows penetration effects on yawing moment to be quite significant. The areas under the two curves indicate the rms value of v_g-induced yawing moment is 73 σ_{v_g} with penetration effects and 33 σ_{v_g} without.

Similarly, Figure 7 indicates that rolling moments due to u_g and w_g are several orders of magnitude less and one order less, respectively, than that due to v_g. Comparison of the two

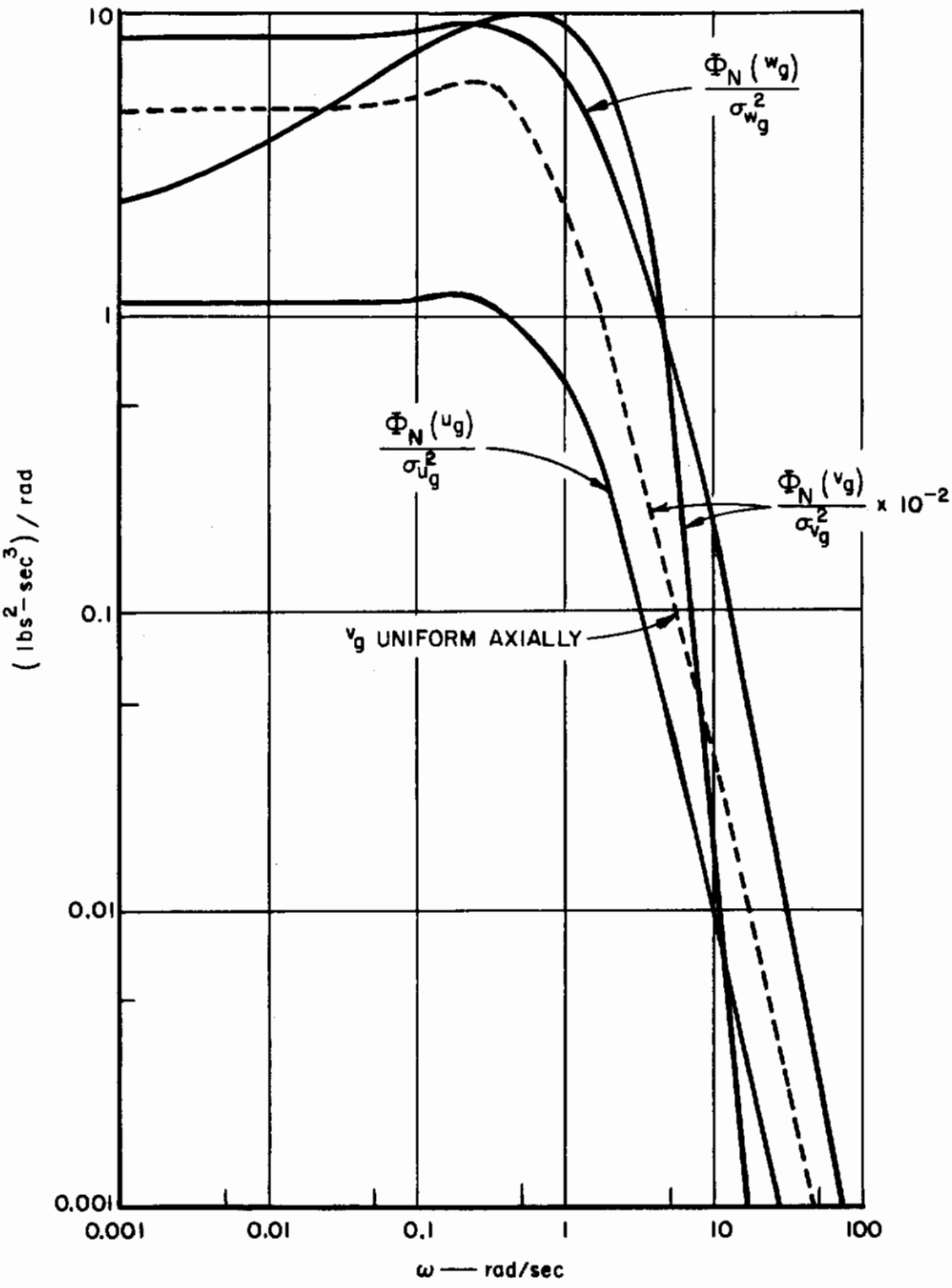

Figure 6. Yawing Moment Power Spectra

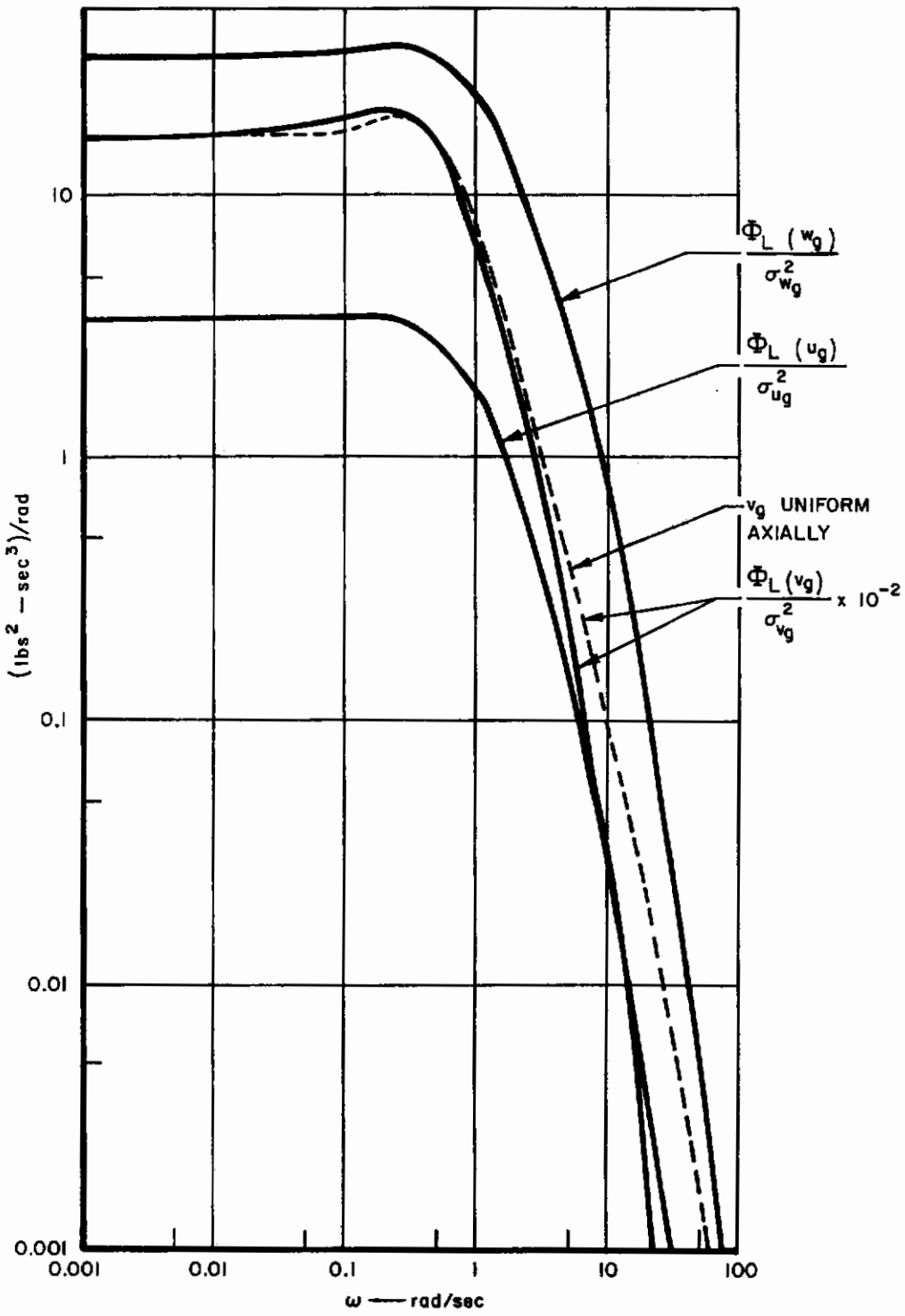

Figure 7. Rolling Moment Power Spectra

$\Phi_{L(v_g)}$ power spectra with and without penetration effects shows penetration effects on rolling moment to be negligible since the curves are nearly coincident below a frequency of 5 rad/sec. The contributions to the rolling moment of the portions of the spectra above 5 rad/sec are negligible.

There is no contribution to side force from u_g and w_g; the contribution from v_g is shown in Figure 8. Again, a comparison of the two $\Phi_{Y(v_g)}$ power spectra shows penetration effects to be negligible in determining the side force power spectral density.

The order-of-magnitude differences between the yawing moment, rolling moment, and side force power spectra due to u_g and w_g spanwise effects, and the power spectra due to v_g allow the significant conclusion that spanwise variations in u_g and w_g are negligible in determining the lateral-directional responses of hovering VTOL aircraft and the gust-induced forces and moments acting thereon. Even wide variations in configuration parameters for various VTOL aircraft will not significantly alter the order-of-magnitude relationships shown above. However, let it be emphasized again that these conclusions are drawn from an analysis based on linear aerodynamic theory which, in turn, says that the gust forces and moments are due to circulation lift and not momentum transfer of energy from the gusts to the vehicle. For hover with low trim angles of attack and/or sideslip angles in less than severe turbulence ($\frac{v_g}{U_o}$ and $\frac{w_g}{U_o}$ less than about 6/25), circulation lift is the predominant mechanism.

Although not a general conclusion, for the VJ-101 analyzed, axial penetration of the lateral gusts, referenced at the center of gravity, is significant only for yawing moments and has a negligible effect in determining rolling moment and side force power spectra for the hovering aircraft.

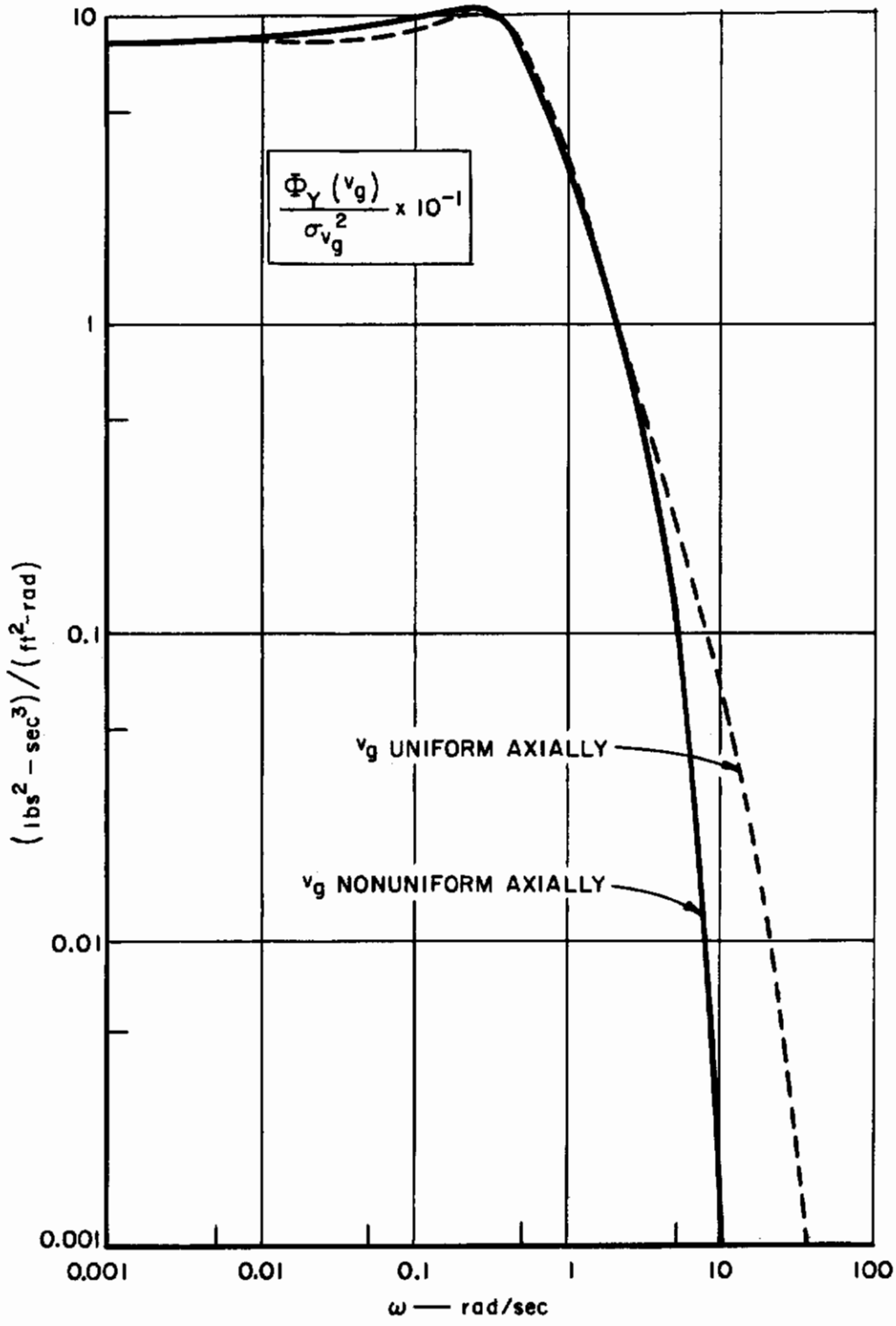

Figure 8. Side Force Power Spectra

SECTION IV

LATERAL-DIRECTIONAL RESPONSE

Now that we have established that only the lateral component of gust velocity need be considered in analyzing the lateral-directional response of the hovering aircraft, matrix Equation (4) reduces to the following three equations for the sideslip, yaw, and roll response angles:

$$\beta = \left[\left(\frac{\beta}{Y}\right)\left(\frac{Y}{v_g}\right)_{FT} + \left(\frac{\beta}{N}\right)\left(\frac{N}{v_g}\right)_{FT} + \left(\frac{\beta}{L}\right)\left(\frac{L}{v_g}\right)_{WT} \right] v_g \tag{49}$$

$$\psi = \left[\left(\frac{\psi}{Y}\right)\left(\frac{Y}{v_g}\right)_{FT} + \left(\frac{\psi}{N}\right)\left(\frac{N}{v_g}\right)_{FT} + \left(\frac{\psi}{L}\right)\left(\frac{L}{v_g}\right)_{WT} \right] v_g \tag{50}$$

$$\phi = \left[\left(\frac{\phi}{Y}\right)\left(\frac{Y}{v_g}\right)_{FT} + \left(\frac{\phi}{N}\right)\left(\frac{N}{v_g}\right)_{FT} + \left(\frac{\phi}{L}\right)\left(\frac{L}{v_g}\right)_{WT} \right] v_g \tag{51}$$

In power spectral density form,

$$\Phi_\beta = \left| \left(\frac{\beta}{Y}\right)\left(\frac{Y}{v_g}\right)_{FT} + \left(\frac{\beta}{N}\right)\left(\frac{N}{v_g}\right)_{FT} + \left(\frac{\beta}{L}\right)\left(\frac{L}{v_g}\right)_{WT} \right|^2 \Phi_{v_g} \tag{52}$$

$$\Phi_\psi = \left| \left(\frac{\psi}{Y}\right)\left(\frac{Y}{v_g}\right)_{FT} + \left(\frac{\psi}{N}\right)\left(\frac{N}{v_g}\right)_{FT} + \left(\frac{\psi}{L}\right)\left(\frac{L}{v_g}\right)_{WT} \right|^2 \Phi_{v_g} \tag{53}$$

$$\Phi_\phi = \left| \left(\frac{\phi}{Y}\right)\left(\frac{Y}{v_g}\right)_{FT} + \left(\frac{\phi}{N}\right)\left(\frac{N}{v_g}\right)_{FT} + \left(\frac{\phi}{L}\right)\left(\frac{L}{v_g}\right)_{WT} \right|^2 \Phi_{v_g} \tag{54}$$

Equations (52), (53), and (54) were evaluated for discrete values of frequency, normalized by the variance or mean square value of v_g, and plotted as the solid curves in Figures 9, 10, and 11. These curves include penetration effects, and $(N/v_g)_{FT}$, $(Y/v_g)_{FT}$, and $(L/v_g)_{WT}$ in the above three equations are as given in Equations (30), (31), and (39). The dashed curves in these figures give the response power spectra without lateral gust penetration effects and were derived from Equations (52), (53), and (54) with the following terms (obtained from Equations (43), (44), and (45) used in place of the frequency-dependent gust transfer functions:

$$\left(\frac{Y}{v_g}\right) = \frac{1}{2} \rho U_o S C_{y_\beta} \tag{55}$$

$$\left(\frac{N}{v_g}\right) = \frac{1}{2} \rho U_o S b C_{n_\beta} \tag{56}$$

$$\left(\frac{L}{v_g}\right) = \frac{1}{2} \rho U_o S b C_{\ell_\beta} \tag{57}$$

Study of Figures 9 through 11 reveals that differences in the response spectra are most pronounced near the closed-loop dutch roll frequency of 1.0 rad/sec. The mean-square values

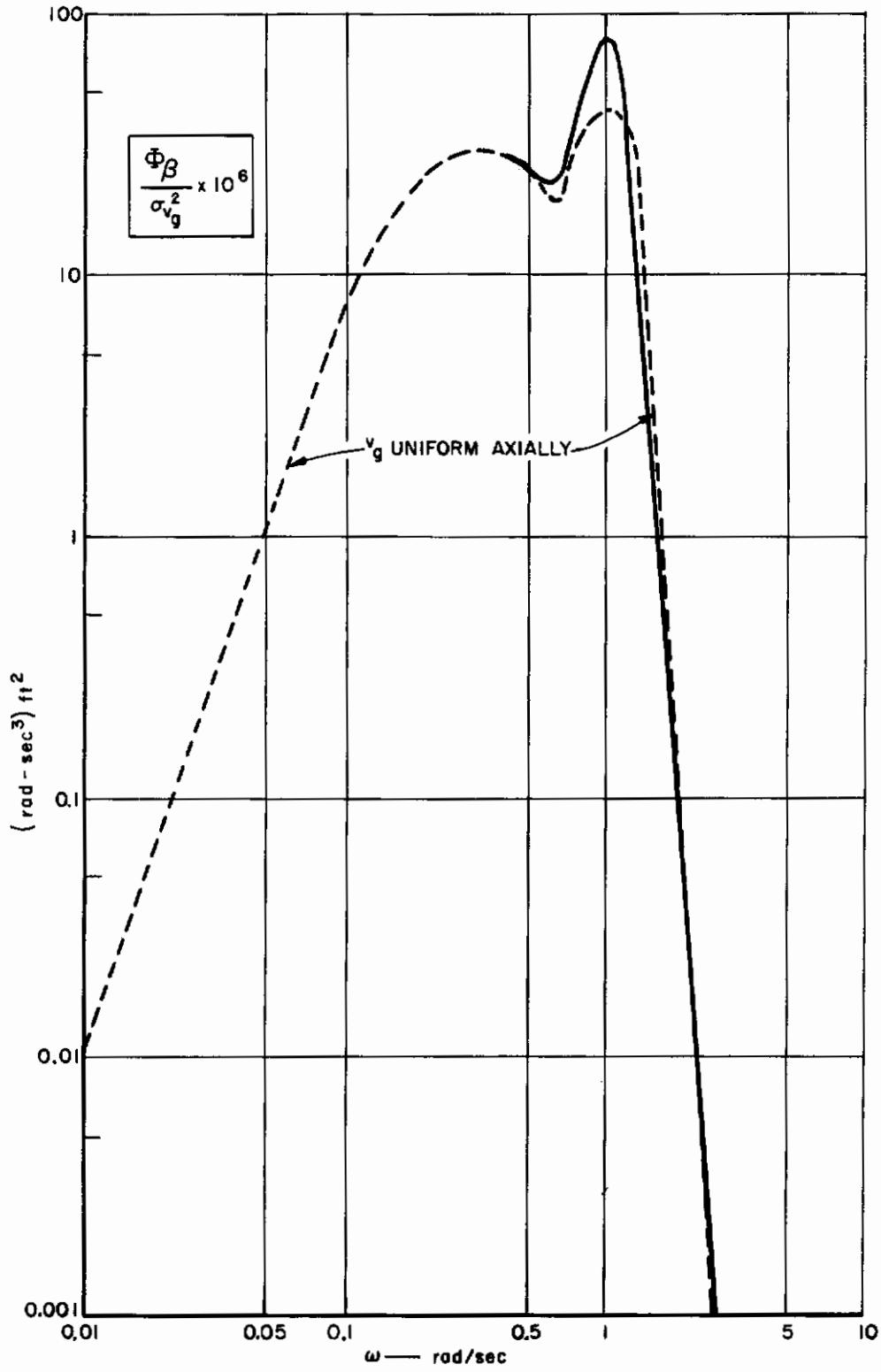

Figure 9. Sideslip Angle Power Spectra

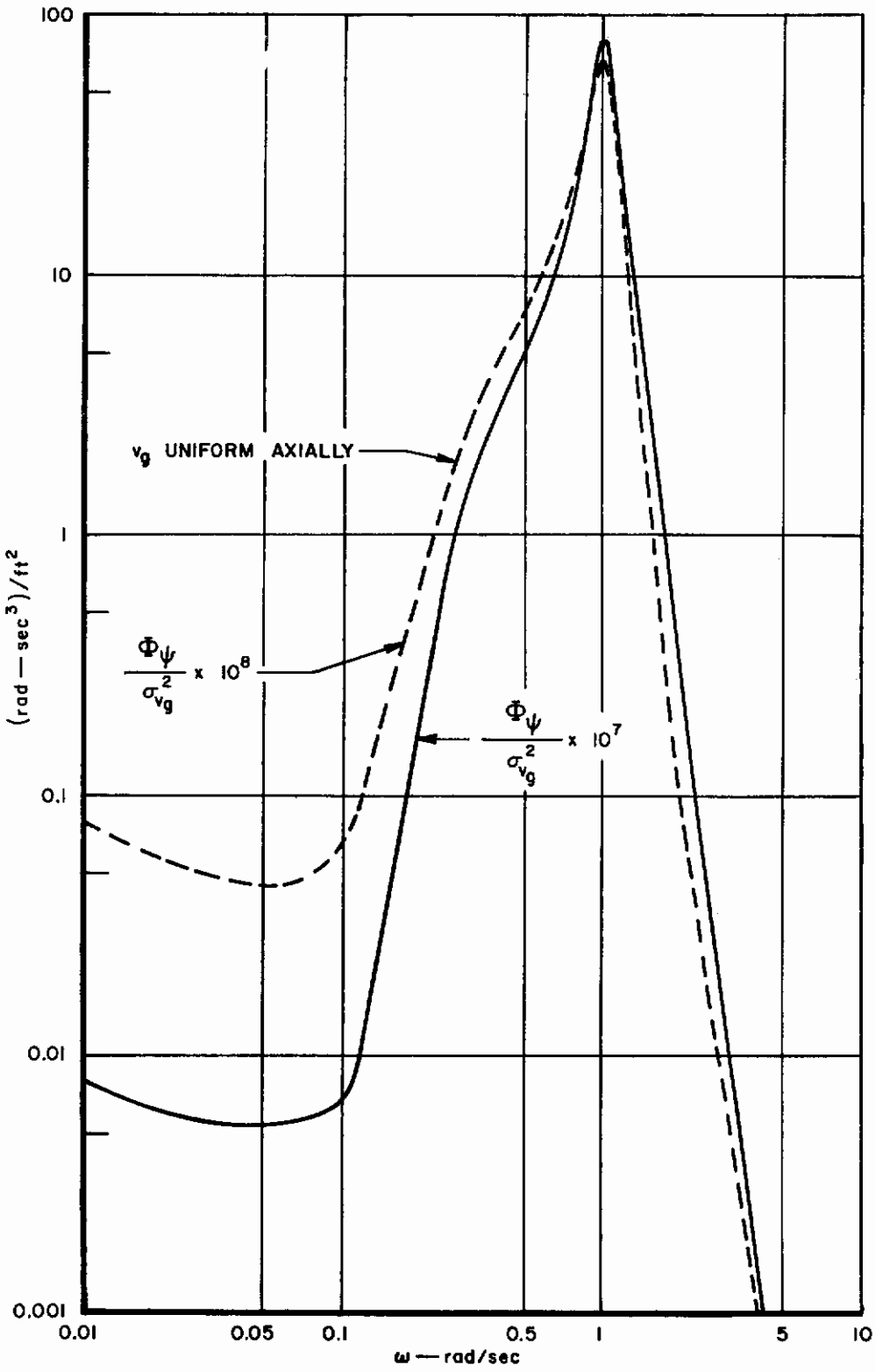

Figure 10. Yaw Angle Power Spectra

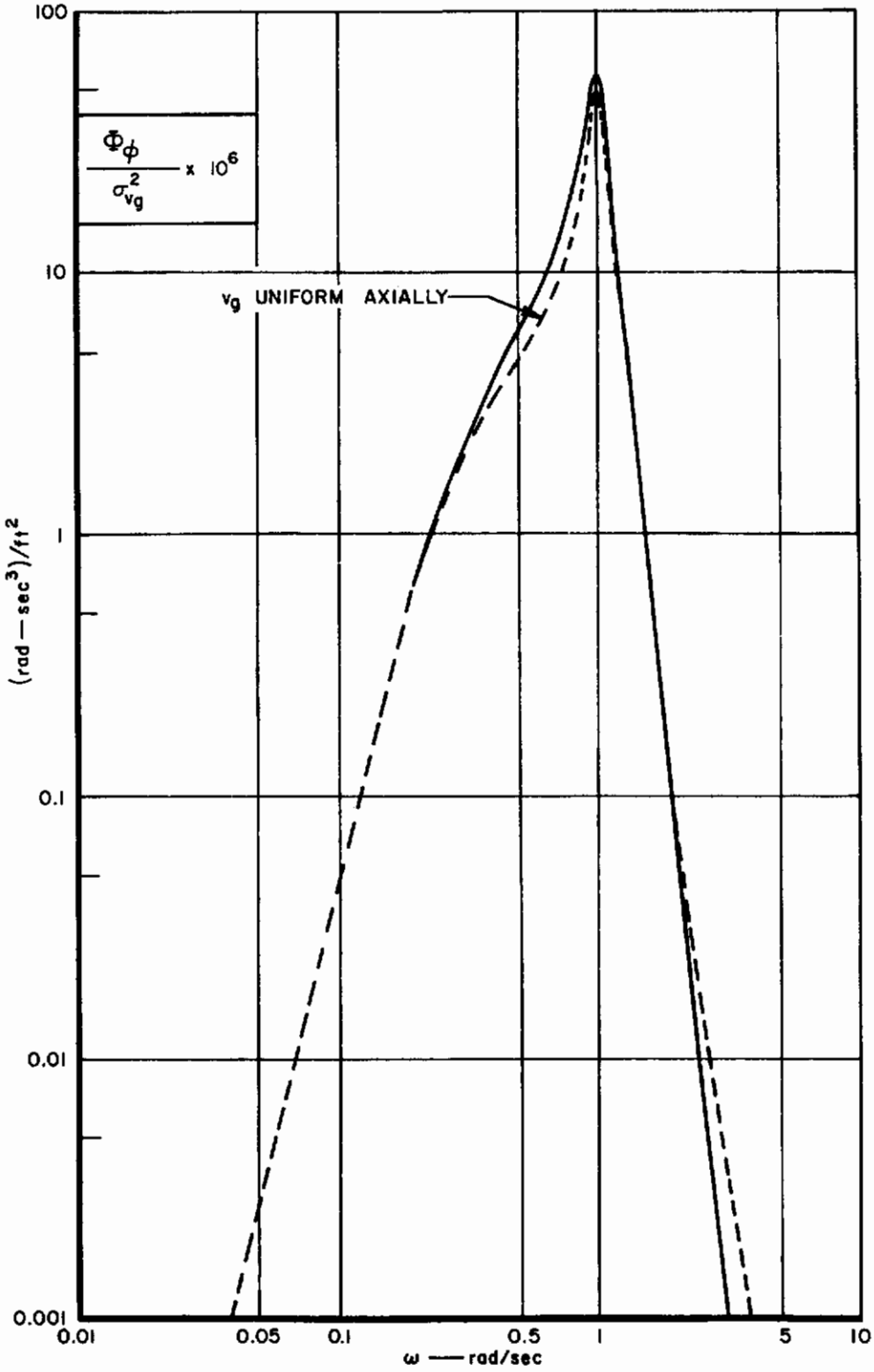

Figure 11. Roll Angle Power Spectra

of β, ψ, and ϕ were obtained by graphically integrating Equations (8), (9), and (10), both with and without (v_g uniform axially) lateral gust penetration effects. With penetration effects:

$$\sigma_\beta^2 = 1.492 \times 10^{-4}\, \sigma_{v_g}^2 \quad ; \quad \sigma_\psi^2 = 12.955 \times 10^{-6}\, \sigma_{v_g}^2 \quad ; \quad \sigma_\phi^2 = 91.17 \times 10^{-6}\, \sigma_{v_g}^2$$

$$\sigma_\beta = 1.222 \times 10^{-2}\, \sigma_{v_g} \quad ; \quad \sigma_\psi = 3.6 \times 10^{-3}\, \sigma_{v_g} \quad ; \quad \sigma_\phi = 9.57 \times 10^{-3}\, \sigma_{v_g}$$

Without penetration effects:

$$\sigma_\beta^2 = 53.1 \times 10^{-6}\, \sigma_{v_g}^2 \quad ; \quad \sigma_\psi^2 = 1.014 \times 10^{-6}\, \sigma_{v_g}^2 \quad ; \quad \sigma_\phi^2 = 73.38 \times 10^{-6}\, \sigma_{v_g}^2$$

$$\sigma_\beta = 7.3 \times 10^{-3}\, \sigma_{v_g} \quad ; \quad \sigma_\psi = 1.008 \times 10^{-3}\, \sigma_{v_g} \quad ; \quad \sigma_\phi = 8.58 \times 10^{-3}\, \sigma_{v_g}$$

The ratios of rms response with penetration effects to rms response without penetration effects are:

$$\sigma_\beta \text{ ratio} = 1.67 \quad ; \quad \sigma_\psi \text{ ratio} = 3.57 \quad ; \quad \sigma_\phi \text{ ratio} = 1.12$$

Thus, on this particular vehicle with the assumed stability augmentation, neglect of penetration effects gives unconservative results for all three response angles.

For a lateral gust intensity (rms value σ_{v_g}) of 6 ft/sec, the rms responses with penetration effects are:

$$\sigma_\beta = 4.20 \text{ deg} \; ; \quad \sigma_\psi = 1.24 \text{ deg} \; ; \quad \sigma_\phi = 3.29 \text{ deg}$$

Without penetration effects:

$$\sigma_\beta = 2.51 \text{ deg} \; ; \quad \sigma_\psi = 0.35 \text{ deg} \; ; \quad \sigma_\phi = 2.95 \text{ deg}$$

SECTION V

CONCLUSIONS AND RECOMMENDATIONS

1. The linear aerodynamic theory used herein is reasonably accurate (about 10% error) for summed trim and gust-induced angles of attack and sideslip angles up to the limit of lift curve slope linearity. For larger trim and gust input angles an approach based on momentum transfer of gust energy to the aircraft should be developed and applied.

2. In the linear aerodynamic range, spanwise variations of longitudinal and vertical components of gust velocity are negligible in determining gust-induced side force, yawing moment, rolling moment, and sideslip, yaw, and roll power spectra and rms response angles for hovering VTOL aircraft. Only the lateral gust velocity component need be considered; and, in general, the axial distribution or penetration effects must be included. The longitudinal dynamics were not considered in this work; however, it seems reasonable that spanwise distributions of u_g and w_g would have even less effect on pitch angle response than they have on roll and yaw response. On the other hand, axial distribution of w_g (penetration effect) would appear to be as significant to pitch response as axial distribution of v_g is to lateral-directional response. It is recommended that these effects on longitudinal response be investigated. The analytical methods described in this report and in the cited references are applicable to the longitudinal case.

3. The power spectra of β, ψ, and ϕ peak in the vicinity of the closed-loop dutch roll natural frequency (1.0 rad/sec in the example presented), and the differences in the spectra with and without v_g penetration effects are greatest at that frequency. Thus, great care should be exercised in calculating the spectra in this region.

4. The analysis methods outlined in this work should be applied to VTOL aircraft in various stages of transition flight to determine the range of flight conditions where spanwise effects of u_g and w_g are no longer negligible.

REFERENCES

1. Etkin, B., "A Theory of the Response of Airplanes to Random Atmospheric Turbulence," Journal of Aero/Space Sci, 26, 409-420 (1959).

2. Eggleston, J. M., and Phillips, W. H., "The Lateral Response of Airplanes to Random Atmospheric Turbulence," NASA TR R-74, pp 41-52 (1960).

3. Bureau of Aeronautics, Navy Dept, Dynamics of the Airframe, Rpt AE-61-4II, Chap II (1952).

4. Eggleston, J. M., and Diederich, F. W., "Theoretical Calculation of the Power Spectra of the Rolling and Yawing Moments on a Wing in Random Turbulence," NACA Rpt 1321 (1957).

5. Eggleston, J. M., "Calculations of the Forces and Moments on a Slender Fuselage and Vertical Fin Penetrating Lateral Gusts," NACA TN 3805 (1956).

UNCLASSIFIED
Security Classification

DOCUMENT CONTROL DATA - R&D
(Security classification of title, body of abstract and indexing annotation must be entered when the overall report is classified)

1. ORIGINATING ACTIVITY (Corporate author)	2a. REPORT SECURITY CLASSIFICATION
Air Force Flight Dynamics Laboratory Wright-Patterson AFB, Ohio 45433	Unclassified
	2b GROUP N/A

3. REPORT TITLE

EFFECTS OF GUST VELOCITY SPATIAL DISTRIBUTIONS ON LATERAL-DIRECTIONAL RESPONSE OF A VTOL AIRCRAFT

4. DESCRIPTIVE NOTES (Type of report and inclusive dates)

Final Report, Oct 1965 - Feb 1967

5. AUTHOR(S) (Last name, first name, initial)

Swaim, Robert L.
Connors, Alonzo J.

6. REPORT DATE	7a. TOTAL NO. OF PAGES	7b. NO. OF REFS
June 1967	34	5

8a. CONTRACT OR GRANT NO.	9a. ORIGINATOR'S REPORT NUMBER(S)
b. PROJECT NO. 8219	AFFDL-TR-67-93
c. Task: 821903 Work Unit 003	9b. OTHER REPORT NO(S) (Any other numbers that may be assigned this report)
d.	

10. AVAILABILITY/LIMITATION NOTICES

Distribution of this document is unlimited. It may be released to the Clearinghouse, Department of Commerce, for sale to the general public.

11. SUPPLEMENTARY NOTES	12. SPONSORING MILITARY ACTIVITY
None	Air Force Flight Dynamics Laboratory Wright-Patterson AFB, Ohio 45433

13. ABSTRACT

The effects of spanwise distribution of longitudinal and vertical components of gust velocity and longitudinal distribution of the lateral component on the lateral-directional response of a hovering VTOL aircraft are analyzed. Results show that spanwise effects of the longitudinal and vertical components are negligible, and the longitudinal distribution of the lateral component is significant in computing the power spectral densities of gust-induced side force, yawing moment, rolling moment, and the aircraft sideslip, yaw, and roll root-mean-square response angles. If the gust-induced angles of attack and sideslip angles are in the nonlinear range of lift curve slope, the above conclusions, which are based on linear aerodynamic theory, may not hold and an analysis based on momentum transfer of gust energy to the aircraft is recommended. Flow field interaction effects due to engine intake and exhaust also were not considered.

DD FORM 1 JAN 64 1473

UNCLASSIFIED
Security Classification

14. KEY WORDS	LINK A		LINK B		LINK C	
	ROLE	WT	ROLE	WT	ROLE	WT
VTOL aircraft Gust response Power spectral density Flight control Automatic control Dynamic response Turbulence						

INSTRUCTIONS

1. ORIGINATING ACTIVITY: Enter the name and address of the contractor, subcontractor, grantee, Department of Defense activity or other organization *(corporate author)* issuing the report.

2*a*. REPORT SECURITY CLASSIFICATION: Enter the overall security classification of the report. Indicate whether "Restricted Data" is included. Marking is to be in accordance with appropriate security regulations.

2*b*. GROUP: Automatic downgrading is specified in DoD Directive 5200.10 and Armed Forces Industrial Manual. Enter the group number. Also, when applicable, show that optional markings have been used for Group 3 and Group 4 as authorized.

3. REPORT TITLE: Enter the complete report title in all capital letters. Titles in all cases should be unclassified. If a meaningful title cannot be selected without classification, show title classification in all capitals in parenthesis immediately following the title.

4. DESCRIPTIVE NOTES: If appropriate, enter the type of report, e.g., interim, progress, summary, annual, or final. Give the inclusive dates when a specific reporting period is covered.

5. AUTHOR(S): Enter the name(s) of author(s) as shown on or in the report. Enter last name, first name, middle initial. If military, show rank and branch of service. The name of the principal author is an absolute minimum requirement.

6. REPORT DATE: Enter the date of the report as day, month, year, or month, year. If more than one date appears on the report, use date of publication.

7*a*. TOTAL NUMBER OF PAGES: The total page count should follow normal pagination procedures, i.e., enter the number of pages containing information.

7*b*. NUMBER OF REFERENCES: Enter the total number of references cited in the report.

8*a*. CONTRACT OR GRANT NUMBER: If appropriate, enter the applicable number of the contract or grant under which the report was written.

8*b*, 8*c*, & 8*d*. PROJECT NUMBER: Enter the appropriate military department identification, such as project number, subproject number, system numbers, task number, etc.

9*a*. ORIGINATOR'S REPORT NUMBER(S): Enter the official report number by which the document will be identified and controlled by the originating activity. This number must be unique to this report.

9*b*. OTHER REPORT NUMBER(S): If the report has been assigned any other report numbers *(either by the originator or by the sponsor)*, also enter this number(s).

10. AVAILABILITY/LIMITATION NOTICES: Enter any limitations on further dissemination of the report, other than those imposed by security classification, using standard statements such as:

(1) "Qualified requesters may obtain copies of this report from DDC."

(2) "Foreign announcement and dissemination of this report by DDC is not authorized."

(3) "U. S. Government agencies may obtain copies of this report directly from DDC. Other qualified DDC users shall request through _____."

(4) "U. S. military agencies may obtain copies of this report directly from DDC. Other qualified users shall request through _____."

(5) "All distribution of this report is controlled. Qualified DDC users shall request through _____."

If the report has been furnished to the Office of Technical Services, Department of Commerce, for sale to the public, indicate this fact and enter the price, if known.

11. SUPPLEMENTARY NOTES: Use for additional explanatory notes.

12. SPONSORING MILITARY ACTIVITY: Enter the name of the departmental project office or laboratory sponsoring *(paying for)* the research and development. Include address.

13. ABSTRACT: Enter an abstract giving a brief and factual summary of the document indicative of the report, even though it may also appear elsewhere in the body of the technical report. If additional space is required, a continuation sheet shall be attached.

It is highly desirable that the abstract of classified reports be unclassified. Each paragraph of the abstract shall end with an indication of the military security classification of the information in the paragraph, represented as *(TS)*, *(S)*, *(C)*, or *(U)*.

There is no limitation on the length of the abstract. However, the suggested length is from 150 to 225 words.

14. KEY WORDS: Key words are technically meaningful terms or short phrases that characterize a report and may be used as index entries for cataloging the report. Key words must be selected so that no security classification is required. Identifiers, such as equipment model designation, trade name, military project code name, geographic location, may be used as key words but will be followed by an indication of technical context. The assignment of links, rules, and weights is optional.